CrossMark

On the Relationship between Magnetic Expansion Factor and Observed Speed of the Solar Wind from Coronal Pseudostreamers

Samantha Wallace[1,2] , C. Nick Arge[2], Nicholeen Viall[2] , and Ylva Pihlström[1,3]
[1] Department of Physics and Astronomy, University of New Mexico, 210 Yale Blvd. NE, Albuquerque, NM 87106, USA
[2] NASA Goddard Space Flight Center, 8800 Greenbelt Rd., Greenbelt, MD 20771, USA

Abstract

For the past 30+ yr, the magnetic expansion factor (f_s) has been used in empirical relationships to predict solar wind speed (v_{obs}) at 1 au based on an inverse relationship between these two quantities. Coronal unipolar streamers (i.e., pseudostreamers) undergo limited field line expansion, resulting in f_s-dependent relationships to predict the fast wind associated with these structures. However, case studies have shown that the in situ observed pseudostreamer solar wind was much slower than that derived with f_s. To investigate this further, we conduct a statistical analysis to determine if f_s and v_{obs} are inversely correlated for a large sample of periods when pseudostreamer wind was observed at multiple 1 au spacecraft (i.e., ACE, STEREO-A/B). We use the Wang–Sheeley–Arge model driven by Air Force Data Assimilative Photospheric Flux Transport (ADAPT) photospheric field maps to identify 38 periods when spacecraft observe pseudostreamer wind. We compare the expansion factor of the last open field lines on either side of a pseudostreamer cusp with the corresponding in situ measured solar wind speed. We find that only slow wind ($v_{obs} < 500\,\mathrm{km\,s^{-1}}$) is associated with pseudostreamers and that there is not a significant correlation between f_s and v_{obs} for these field lines. This suggests that field lines near the open–closed boundary of pseudostreamers are not subject to the steady-state acceleration along continuously open flux tubes assumed in the f_s–v_{obs} relationship. In general, dynamics at the boundary between open and closed field lines such as interchange reconnection will invalidate the steady-state assumptions of this relationship.

Unified Astronomy Thesaurus concepts: Solar wind (1534); Solar corona (1483); Solar coronal streamers (1486)

1. Introduction

The solar wind is a result of the supersonic expansion of hot ($T \sim 10^6\,\mathrm{K}$) plasma and magnetic field in the solar corona. This highly ionized plasma with coronal magnetic fields frozen into it flows out into the heliosphere, with observed speeds (v_{obs}) ranging between ~250 and 750 km s^{-1} (Feldman et al. 1978). This outflow can be approximated in models as originating from regions on the Sun that have largely unipolar magnetic fields and are magnetically "open" (i.e., flux tubes with only one footpoint connected to the Sun), or coronal holes. Coronal holes have a lower temperature and density relative to the background corona and are thus identified in remote coronal observations by their reduced X-ray and extreme ultraviolet (EUV) emission. It is important to note that the boundaries of coronal holes observed remotely may not be precisely where the magnetic open–closed boundaries are located (de Toma et al. 2005).

How the solar wind is accelerated is an area of active research, in which theory and empirical relationships are heavily relied upon. Thirty years ago, Wang & Sheeley (1990) discovered an inverse relationship between solar wind speed (as measured by spacecraft near Earth) and the coronal field line expansion at the location that the observed solar wind emerged from. Using a magnetostatic potential field source surface (PFSS) model (Altschuler & Newkirk 1969; Schatten et al. 1969; Wang & Sheeley 1992), they extrapolated the coronal field out to 2.5 $R_\odot$ (Hoeksema et al. 1983) from photospheric field observations at 1 $R_\odot$ and quantified the rate of inferred expansion of a coronal magnetic flux tube compared

to an R^{-2} drop-off with the following equation:

$$f_s = \left(\frac{R_{ph}}{R_{ss}}\right)^2 \left(\frac{B_{ph}}{B_{ss}}\right), \tag{1}$$

where B_{ph} and B_{ss} are the field strengths along each flux tube at the photosphere ($R_{ph} = 1\,R_\odot$) and source surface ($R_{ss} = 2.5\,R_\odot$), respectively (Wang & Sheeley 1992). By tracing model-derived magnetic field lines from the Earth back to the Sun, they found that fast solar wind ($v_{obs} > 500\,\mathrm{km\,s^{-1}}$) is correlated with the centers of coronal holes where f_s is small, while slow solar wind ($v_{obs} < 500\,\mathrm{km\,s^{-1}}$) originates from coronal hole boundaries where f_s is large. This discovery was an important breakthrough, as it provided the heliophysics community with a way to both predict and forecast the solar wind (Arge & Pizzo 2000; Pizzo et al. 2011).

While the practical importance of the inverse relationship between observed solar wind speed and expansion factor is without dispute (Sheeley 2017), the physical interpretation and relevance behind it has been debated ever since. In wave turbulence–driven (WTD) acceleration theories, energy deposited into the corona is a function of a flux tube's radius. Thus, differences in observed solar wind speed are attributed to the rate of flux tube expansion in the low corona, implying a physical connection between f_s and v_{obs}. This is supported by quantitative theoretical arguments and modeling using steady-state, continuously open flux tubes (Wang et al. 1996; Cranmer et al. 2007). In addition to speed, steady-state models are generally able to replicate long-term empirical trends between f_s and solar wind density, Alfvénicity, and charge state (Wang & Sheeley 2003; Cranmer et al. 2007; Wang et al. 2009; Cranmer 2010).

In contrast, reconnection/loop-opening (RLO) theories argue that the magnetic reconnection of open field lines with closed magnetic loops imparts both the energy and mass flux needed into the overlying corona to obtain the terminal speed of the solar wind (Fisk 2003). This theory assumes a fixed energy deposition at the coronal base, as opposed to depositing energy per unit volume as a function of radius as in WTD and flux tube expansion–based models. Fisk (2003) argued that slow wind emerges from coronal hole boundaries where there is access to larger, denser closed loops from within streamers and fast wind emerges from deep inside coronal holes where there is only access to very small loops. Thus, he asserted that the existence of the f_s–v_{obs} relationship is simply a coincidence due to the magnetic topology of the closed magnetic field. The RLO theories are also generally able to reproduce long-term trends between observed speed, density, and charge states (Schwadron et al. 1999; Fisk 2003). These theories additionally provide an explanation for the first ionization potential (FIP) enhancement observed in some slow wind observations (Geiss et al. 1995; Zurbuchen et al. 1998). However, there is a growing understanding in the heliophysics community that WTD and RLO acceleration theories are not mutually exclusive, so determining which theory plays a dominant role and under what circumstances is essential to progress (Cranmer 2009; Viall & Borovsky 2020).

Similarly, Riley et al. (2001) developed an alternative empirical relationship that predicts solar wind speed based on the minimum angular separation between the solar wind source (i.e., open field line footpoint) and the nearest open–closed boundary at $1\,R_\odot$, or the "coronal hole boundary distance" (DCHB or θ_b). In this relationship, when a field line has a small θ_b, its footpoint is close to the open–closed boundary, and the solar wind speed is slow. While the empirical relationship between θ_b and v_{obs} is not inherently physical, a major difference between this relationship and f_s–v_{obs} relationships is that it could be a proxy for magnetic reconnection. It also does not constrain the magnetic field lines to being continuously open.

Periods for which f_s-dependent empirical relationships have performed poorly are when the in situ observed solar wind was formed at a coronal unipolar streamer. Otherwise known as pseudostreamers, these solar magnetic structures differ from their dipolar counterparts (i.e., helmet streamers) in that they form from two converging coronal hole boundaries of the same polarity and therefore do not form a current sheet. Instead, these field lines converge above the cusp (i.e., X-point) and limit the expansion of the underlying closed field (Wang et al. 2012). Thus, pseudostreamers in theory would have smaller expansion factors than helmet streamers, leading Wang et al. (2007) to originally postulate that pseudostreamer wind was fast. However, Riley & Luhmann (2012) used a global MHD coronal model to identify a period when ACE was well positioned to observe the solar wind that emerged from a pseudostreamer. They found that the observed solar wind was slow, yet the predicted speed based on the original Wang–Sheeley (WS) relationship was fast due to the low expansion factors associated with this structure. This work was expounded on in Riley et al. (2015) to test the use of both f_s and θ_b to predict solar wind speed. They found that on average, empirical relationships relying either solely or mostly on θ_b outperform the original WS f_s–v_{obs} relationship, especially when pseudostreamers are present. They concluded that θ_b

predicts solar wind speed better than f_s and suggested that their findings may rule out a causal relationship between solar wind speed and f_s (or at least relegate it to a minor role). However, both studies only investigated in detail one particular Carrington rotation where a well-defined pseudostreamer was observed (CR 2060).

In this study, we build upon the work of Riley & Luhmann (2012) and Riley et al. (2015) and investigate the relationship between expansion factor (f_s, as originally defined by Wang & Sheeley 1990) and observed solar wind speed for several periods when multiple 1 au spacecraft (ACE, STEREO-A, STEREO-B) observe pseudostreamer wind. We exploit the rigorous capabilities of the Wang–Sheeley–Arge (WSA) model (Arge & Pizzo 2000; Arge et al. 2003; Arge et al. 2004) coupled with Air Force Data Assimilative Photospheric Flux Transport (ADAPT; Arge et al. 2010, 2011, 2013; Hickmann et al. 2015) photospheric field maps and develop a methodology to determine the precise source regions of the in situ observed solar wind. This methodology is used to identify periods when the observed solar wind emerged from the last two model-derived open field lines converging at a pseudostreamer X-point, where the spacecraft connectivity changes from one coronal hole boundary to another of like polarity. The individual model-derived solar wind parcel that emerges from each field line is then propagated outward to an observing spacecraft, and the model-predicted arrival time is used to record the in situ observed solar wind speed. This observed speed is then compared to the corresponding expansion factor. We perform a statistical analysis over all identified field lines to examine whether expansion factor and observed solar wind speed are correlated for periods when pseudostreamer wind is observed.

This paper is structured as follows. Section 2 gives an overview of the ADAPT–WSA model and outlines the methodology used to identify periods when spacecraft observe pseudostreamer wind. The results are presented in Section 3. They are then discussed in the context of other empirical solar wind speed relationships and solar wind formation theories in Section 4 and summarized in the final section.

2. Identifying in situ Observed Pseudostreamers with ADAPT–WASA

In this section, the ADAPT–WSA model is summarized, and the methodology we developed to identify periods when spacecraft sample the solar wind that emerged from pseudostreamers is outlined in detail. While this methodology is applied to pseudostreamers in this work, it can also be used to investigate solar wind that originates from other sources (e.g., helmet streamers, coronal holes, plasma originating from or near active regions (ARs)).

2.1. The ADAPT–WSA Model

The WSA model is a combined empirical- and physics-based model that is an improved version of the original WS model (Wang & Sheeley 1992, 1995). The WSA model relies on input global photospheric field maps assembled from full-disk observations of the solar photospheric magnetic field (i.e., magnetograms). These maps are constructed in a variety of ways representing either a time history of central meridian evolution over a Carrington rotation (i.e., diachronic) or, more preferably, one moment in time (i.e., synchronic). Given the

current lack of far-side solar magnetic field observations and the poor observations of the poles, global synchronic representations of the photospheric magnetic field are only possible through flux-transport models (Worden & Harvey 2000; Schrijver & de Rosa 2003). In this work, we use global synchronic photospheric field maps generated by the ADAPT model. The ADAPT model utilizes magnetic flux transport based on the Worden & Harvey (2000) model to account for differential rotation, along with meridional and supergranulation flows, when observational data are not available. In addition, ADAPT incorporates new magnetogram input using the ensemble least-squares data assimilation technique accounting for both model and data uncertainties as the maps are generated (Hickmann et al. 2015). For example, ADAPT heavily weights observations taken near the disk center, where magnetograms are most reliable, while the model specification of the field is generally given more weight near the limbs, where observations are the least reliable. ADAPT produces an ensemble of maps (or realizations) for any given moment in time that ideally represents the uncertainty in the global photospheric magnetic field distribution.

Using ADAPT maps (e.g., middle panel of Figure 1) as input, WSA derives the coronal field using a coupled set of potential field–type models. The first is a traditional PFSS model, which determines the coronal field out to the source surface height. The traditional source surface height of 2.5 $R_\odot$ (Hoeksema et al. 1983) is used in this study because it has been shown in prior work to produce good agreement between WSA-derived open flux and that derived from helium and EUV coronal hole observations over nearly two solar cycles (Wallace et al. 2019) with the same set of vector spectromagnetograph (VSM; Henney et al. 2009) magnetograms used in this study. The output of the PFSS model serves as input to the Schatten current sheet (SCS) model (Schatten 1971), which provides a more realistic magnetic field topology of the upper corona. Although this solution extends out to infinity, WSA uses a portion of the coronal field solution that terminates at an outer boundary radius set by the user (5 $R_\odot$ for this work). The following empirical velocity relationship is then used to determine the solar wind speed of each magnetic field line at the outer boundary:

$$v(f_s, \theta_b) = 285 + \frac{685}{(1 + f_s)^{2/9}} \{1 - 0.8e^{-(\theta_b/2)^2}\}^3, \quad (2)$$

which is a function of both the expansion factor and the minimum angular separation between an open field line footpoint at 1 $R_\odot$ and the nearest open–closed boundary. Instead of "back-mapping" a spacecraft to the outer boundary of the model, WSA propagates solar wind parcels outward from the endpoints of each field line located at 5 $R_\odot$ to an observing spacecraft (i.e., ACE or STEREO-A/B in this study). Stream interactions are accounted for in the solar wind propagation using a simple 1D modified kinematic model, which prevents fast streams from bypassing slow ones (Arge et al. 2004). When coupled with ADAPT, WSA derives an ensemble of 12 solutions, each representing the global state of the coronal field and connectivity from a spacecraft to 1 $R_\odot$ for a given moment in time. The best realization is then determined by comparing the model-derived and observed interplanetary magnetic field (IMF) and solar wind speed.

Since WSA uses a magnetostatic coronal model, it is not possible for the model to capture the Sun's time-dependent phenomena associated with the opening and closing of magnetic flux. While we can account for time-dependent photospheric phenomena with ADAPT, WSA only derives the magnetic connectivity between an observing spacecraft and model-derived field lines that are open. Similarly, WSA cannot provide information regarding how long a particular field line has been open. Therefore, when the model predicts that a spacecraft measured plasma near a closed-flux system (i.e., the open–closed boundary), the two physical scenarios that are possible are that the plasma originated (1) from that particular open field line or (2) on a closed field that was recently opened via interchange reconnection, whereas ADAPT–WSA cannot make the distinction between the two possible scenarios.

2.2. Methodology

Figures 1–3 present one period when the solar wind that emerged from a pseudostreamer (highlighted in green in all three figures) is observed by STEREO-A and are used to illustrate the methodology of this work. We first use the ADAPT–WSA model to derive the global coronal field (bottom panel of Figure 1), as well as the connectivity between the projection of STEREO-A's location at 5 $R_\odot$ and the open field footpoints at 1 $R_\odot$ (top panel of Figure 1). Throughout Figure 1, dates labeled in red above the white/red tick-marks (i.e., subsatellite points; see Figure 1 for definition) correspond to when and where the solar wind *left* the Sun at 5 $R_\odot$, as opposed to when it *arrived* at STEREO-A. Similarly, black lines extend from the subsatellite track to 1 $R_\odot$, revealing the model-derived source regions of the solar wind that ultimately was observed at STEREO-A. The connectivity plots (e.g., top panel of Figure 1) are used to identify periods when the in situ observed solar wind was formed at a pseudostreamer by searching for instances when the spacecraft connectivity (i.e., black lines) changes from one coronal hole boundary to another of the same polarity (indicated in gray scale). The top panel of Figure 1 reveals that on 2014 July 12, STEREO-A was magnetically connected to the boundaries of two mid-latitude coronal holes of positive polarity, shown with green lines that connect the subsatellite track (i.e., white crosshairs) to either coronal hole. Thus, on July 12, the solar wind emerged from this specific location as derived by ADAPT–WSA and propagated outward to eventually be observed at STEREO-A ∼4–6 days later. The bottom panel of Figure 1 further confirms that the STEREO-A subsatellite track is embedded entirely in positive field at 5 $R_\odot$ for the days surrounding July 12.

Before investigating the specific field lines of each pseudostreamer that are connected to a spacecraft, the best ADAPT–WSA solution of the 12 must be selected for each period of interest. To do so, we compare the WSA-derived solar wind speed and IMF polarity for all 12 realizations with observations from ∼4–6 days after the solar wind left the Sun (i.e., approximate travel time of the solar wind to 1 au). The best realization for the pseudostreamer identified in Figure 1 is shown in Figure 2, which compares the model-derived (blue) and STEREO-A observed (black) solar wind speed and IMF for a portion of CR 2152 (approximately 2 weeks). For the days surrounding the estimated time of arrival of the pseudostreamer wind at STEREO-A (i.e., July 17–19), the model-derived solar wind speed and IMF agree well with that observed at STEREO-A. While there are other instances during this CR
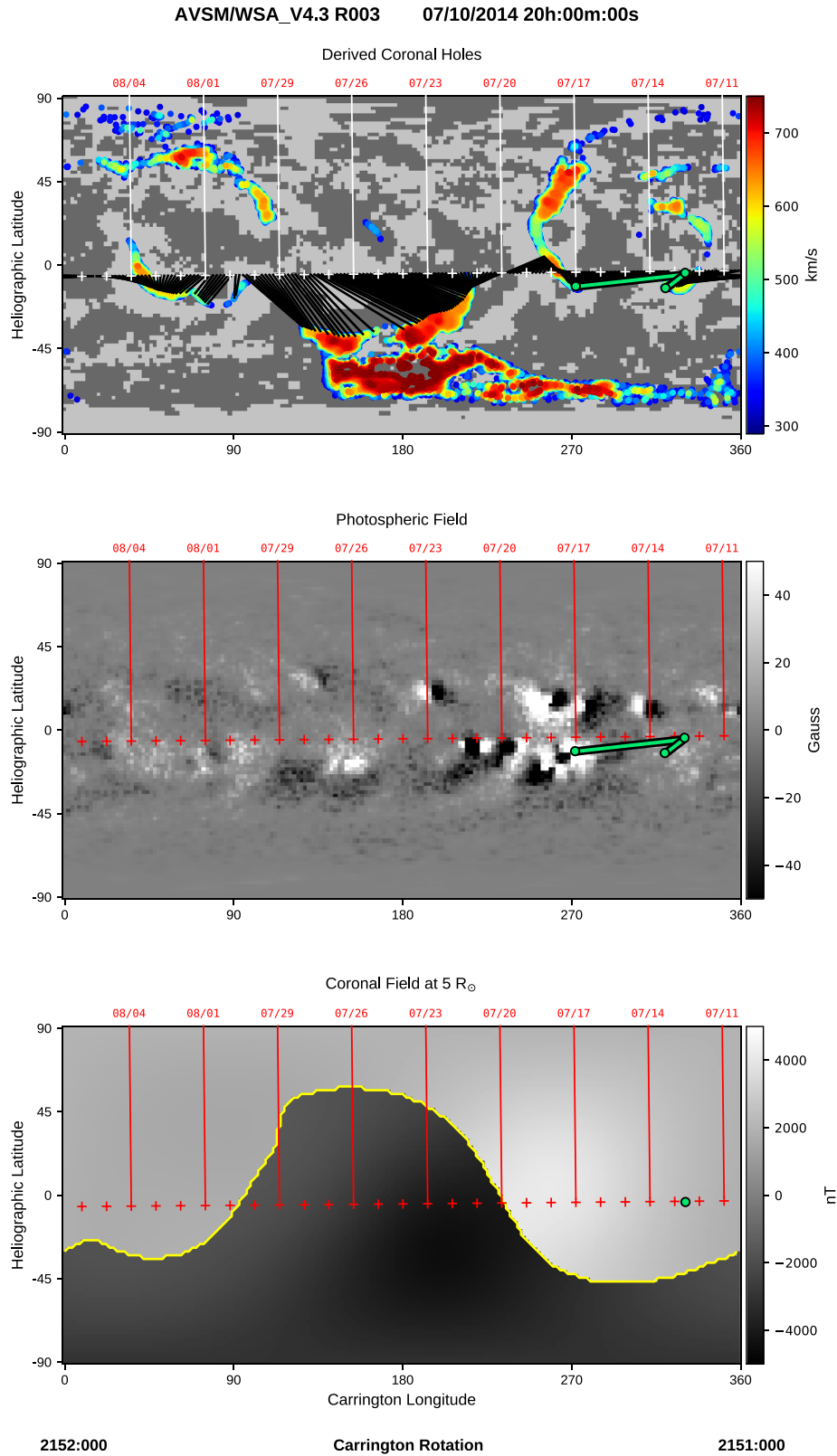
Figure 1. ADAPT–WSA model output for CR 2152 (2014 July–August). White (top panel) and red (middle and bottom panels) tick-marks label the subsatellite points, representing the back-projection of STEREO-A's location at 5 $R_\odot$, with dates labeled above in red. (Top) WSA-derived open field at 1 $R_\odot$ with model-derived solar wind speed in color scale. The field polarity at the photosphere is indicated by the light/dark (positive/negative) gray contours. Black lines show the magnetic connectivity between the projection of STEREO-A's location at 5 $R_\odot$ and the solar wind source region at 1 $R_\odot$. Two green lines mark where STEREO-A samples the solar wind that emerged from a pseudostreamer (i.e., the STEREO-A connectivity changes from one coronal hole boundary to another of the same (outward) polarity). (Middle) Synchronic ADAPT-VSM photospheric field (Gauss) for 2014 October 7 00:00:00 UTC, which reflects the time stamp of the last magnetogram assimilated into this map. See the top panel for a description of the two green lines. (Bottom) WSA-derived coronal field at 5 $R_\odot$. The yellow contour marks the model-derived heliospheric current sheet, where the overall coronal field changes sign.
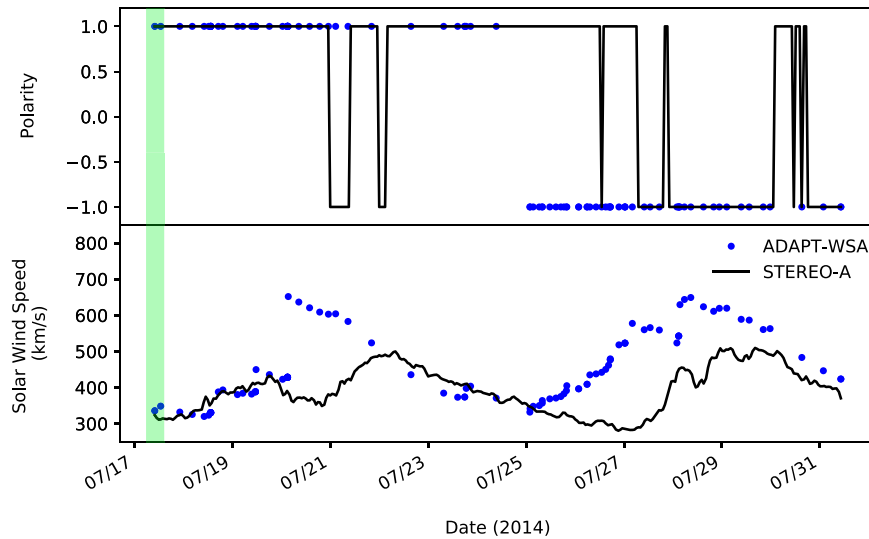
Figure 2. ADAPT–WSA model output (blue) vs. STEREO-A observations (black) for approximately 2 weeks during CR 2152. Each blue dot represents an individual solar wind parcel that connects to STEREO-A, as derived by the model. The highlighted portion in green contains the model output for two solar wind parcels, one that emerged from the two last open field lines forming the pseudostreamer cusp identified in Figures 1 and 3. (Top) polarity and (bottom) solar wind speed.

where the model did not accurately derive the solar wind speed (i.e., July 21, July 25–30), the model-derived parameters for the days surrounding the period of interest agree well. This gives us confidence in the model-derived connectivity between solar wind parcels propagated out from pseudostreamer field lines and STEREO-A. Since ADAPT produces photospheric field solutions for a fixed moment in time, maps used within a few days of each period of interest generally produce the most realistic solutions, whereas a different methodology would be necessary to obtain good agreement with observations over an entire CR. Plots such as Figure 2 are generated for all 12 realizations and initially used to quickly determine the most realistic model solution for the time period of interest. This plot is revisited in greater detail later in this section.

We then use 3D visualization software (GeospaceX 2015) to overplot field line extrapolations of the best ADAPT–WSA realization for each period of interest onto the photosphere (e.g., Figure 3). This allows us to identify the specific field lines that the in situ observed pseudostreamer wind emerged from. This software provides the location of each field line footpoint at $1\,R_\odot$ and endpoint at $5\,R_\odot$, allowing us to obtain model-derived parameters specific to each field line, such as expansion factor and solar wind speed. Figure 3 shows a subset of open magnetic field lines plotted in triads for CR 2152. The 3D rendering tool allows the user to display this particular subset of field lines, which includes only those magnetically connected to the STEREO-A subsatellite points at $5\,R_\odot$ and those located a half a grid cell above and below. The middle field lines in each triad correspond to the black lines that map to the white crosshairs (i.e., STEREO-A subsatellite track) in the top panel of Figure 1 and are thus the source of each solar wind parcel observed by the spacecraft. Figure 3 shows these field lines as viewed in the ecliptic plane in panel (a) and from the solar north pole in panel (b). The two sets of field lines highlighted in green in Figure 3 show where STEREO-A traversed this pseudostreamer by revealing when STEREO-A changed connectivity from one coronal hole boundary to another of like polarity. These same field lines correspond to the two green lines in the top panel of Figure 1. Once the last open field lines are identified for each pseudostreamer, we

obtain the corresponding expansion factors. It is important to note that since we are investigating pseudostreamers observed in situ, observations and field line modeling of each structure only represent a 2D slice of a larger 3D structure.

The model also assigns a solar wind speed (Equation (2)) to individual solar wind parcels that emerge from each field line along the subsatellite track (i.e., middle field lines in the triads in Figure 3). These parcels are propagated outward by the model to the observing spacecraft. Their model-determined arrival time is then used to identify the STEREO-A observed solar wind speed. Figure 2 highlights the model-estimated arrival time at STEREO-A of the solar wind that emerged from the pseudostreamer identified in Figures 1 and 3 (all shown in green). Each blue dot in Figure 2 represents the model-derived solar wind speed and IMF for an individual solar wind parcel propagated out from a specific source region (i.e., field line) of the STEREO-A observed solar wind (Figure 3). The two solar wind parcels that originated from the last two open field lines identified in Figures 1 and 3 (both highlighted in green) were observed at STEREO-A between 10:00:00 and 13:30:00 UTC on 2014 July 17, as determined by WSA. For this time period, the model-derived and STEREO-observed IMF polarity and solar wind speed are in good agreement. In this study, we did not include periods when WSA produced incorrect polarity or the model-derived and spacecraft-observed solar wind speeds differ by more than 0.5 day in arrival time. This window is selected because it approximately corresponds to the typical uncertainty of WSA's solar wind speed predictions of ±0.5 day (Owens et al. 2005). We also did not include periods in which coronal mass ejections (CMEs) were identified in situ (Richardson 2014).

Using the above methodology, we investigate over a decade's worth of observations to identify periods when various spacecraft (ACE, STEREO-A/B) observed the solar wind that emerged from pseudostreamers. We first use diachronic VSM photospheric field maps (i.e., one map for each Carrington rotation) as input into WSA to derive the coronal field for CR 2025–2185 (2005 January–2016 December). This provided a quick way to scan through years of model-derived connectivity for the three different spacecraft
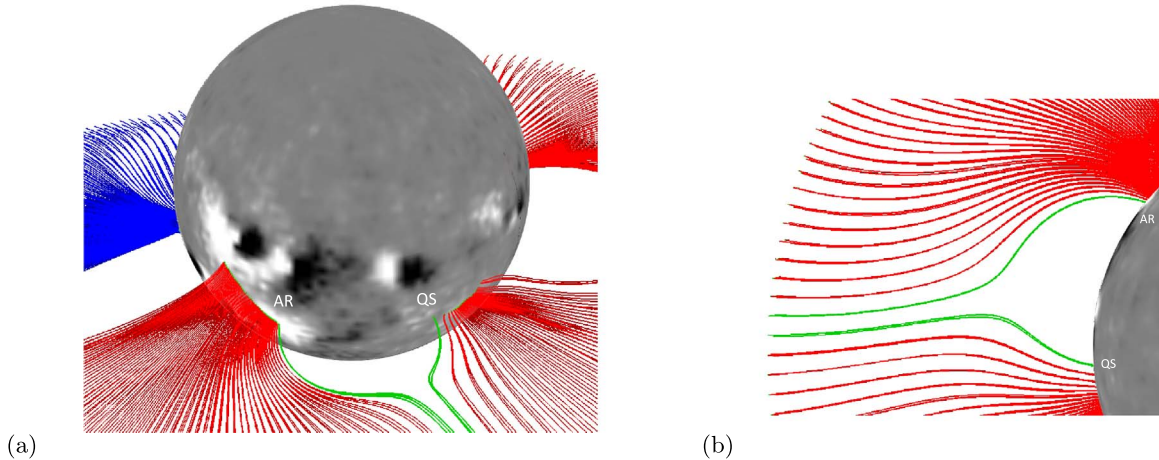
(a)   (b)

Figure 3. A 3D rendering of STEREO-A subsatellite point magnetic connectivity to 1 $R_\odot$ for 2014 July 11–August 6. These dates correspond to when the solar wind left the Sun at 5 $R_\odot$. Plotted are 180 triads of magnetic field lines at 2° resolution, which include the sources of the observed solar wind at STEREO-A (in the middle of each triad), surrounded by those positioned half a grid cell above and below. Red (blue) lines denote outward (inward) polarity. The type of magnetic field on either side of the pseudostreamer null point is labeled (i.e., "QS" for quiet Sun and "AR" for active region). The last open field lines converging to the pseudostreamer X-point are shown in green and viewed from (a) the ecliptic plane and (b) the solar north pole.

(e.g., top panel of Figure 1) and search for periods when spacecraft could have observed pseudostreamer wind. We then use ADAPT-VSM synchronic maps surrounding each period of interest to drive WSA and produce instantaneous global coronal solutions. In total, we identify 38 unambiguous cases where spacecraft sampled the solar wind that emerged from pseudostreamers.

For each pseudostreamer, we compare the observed solar wind speed and expansion factor for each of the last two open field lines converging at the X-point separately (e.g., Figure 3, shown in green). These field lines trace back to two different coronal holes, and their footpoints can be grounded in entirely different types of magnetic field back at the Sun—either in quiet Sun (QS) or an AR. An example is shown in Figure 3, where there is asymmetric expansion on either side of the null point (Figure 3(b)). Table 1 compares the expansion factor, photospheric field magnitude, and observed solar wind speed for the last open field lines forming this structure (Figure 3, shown in green). The order-of-magnitude difference in the magnetic expansion factor is attributed to one field line being rooted in an AR (larger f_s) and the other in QS (smaller f_s). By treating each separately, we preserve the expansion history of each field line on either side of the null point.

3. Results

Figure 4 compares the observed solar wind speed versus expansion factor for all individual last open field lines forming the pseudostreamers identified with the methodology outlined in Section 2.2. The observed photospheric field strength at each field line footpoint is also shown in color scale. In Figures 4–7, the observed speed of each solar wind parcel is an average of the hourly data over ±0.5 day surrounding when the model-derived parcel arrived at the observing spacecraft. We averaged in this way to account for the ±0.5 day uncertainty window in the model-derived solar wind parcel arrival time, discussed in Section 2.2. Represented in Figure 4 are 38 pseudostreamers and 76 field lines in total (i.e., two for each pseudostreamer). This event list spans from the end of solar cycle 23 through most of cycle 24, with pseudostreamers that form at various

Table 1
Field Lines in Figure 3

	Field Line in AR	Field Line in QS
$\|B_{\mathrm{ph}}\|$ (G)	195.1	10.8
f_s	260.8	14.9
v_{obs} (km s^{-1})	326	321

locations on the disk during both minimum and maximum periods (for a complete list, see the Appendix). One notable result that is that the solar wind that originates from these field lines is slow (280 km s^{-1} < v_{obs} < 500 km s^{-1}). This is in agreement with prior studies (Crooker et al. 2012; Riley & Luhmann 2012; Wang et al. 2012) that showed that the in situ observed pseudostreamer wind is slow for the cases identified in their study. Our results suggest that the observed speed of the solar wind that emerges from these structures is generally slow.

In order to investigate the relationship between the expansion factor and speed of the solar wind that emerges from each pseudostreamer field line, we calculated the Pearson correlation coefficient (PCC) for these two quantities and report them in Table 2. Table 2 also lists the p-value associated with each correlation coefficient, which represents the probability that the correlation occurred at random. The PCC for all field lines in this study (i.e., those included in Figure 4) is −0.1075, with approximately a one-in-three probability that this result occurred by chance, implying that there is no statistically significant correlation between f_s and v_{obs} for this data set. A linear regression was also calculated and included in Figure 4, but it is not likely to have any significance. This result is consistent with prior work (Riley & Luhmann 2012; Riley et al. 2015), which investigated the relationship between f_s and v_{obs} for in situ observed pseudostreamers but only focused on one period in detail (CR 2060). In these studies, f_s-dependent empirical relationships overestimated the observed pseudo-streamer solar wind speed. In our study, we use a more robust approach to identify the in situ observed pseudostreamer wind
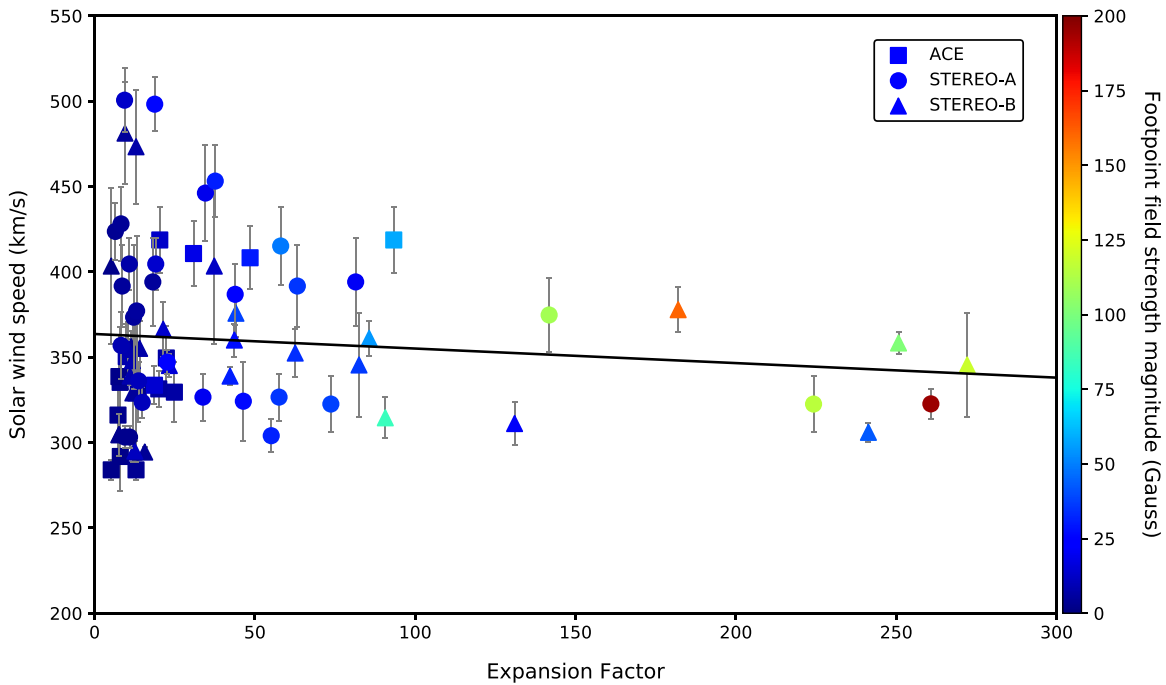
Figure 4. Observed solar wind speed vs. expansion factor for all 76 individual last open field lines of the 38 identified pseudostreamers. Each pseudostreamer is represented by two field lines, one from each coronal hole boundary, which together form the 2D slice of a pseudostreamer that was observed by ACE, STEREO-A, or STEREO-B (denoted by different shapes in the legend). The observed solar wind speed is averaged over ±0.5 day from the WSA-derived solar wind parcel time of arrival at the spacecraft. Error bars in gray represent the standard deviation in observed solar wind speed over a 1 day bin, centered on the time (as determined by WSA) that the pseudostreamer wind was measured at each spacecraft. The black line denotes the calculated linear regression for this data set.

over a large, comprehensive sample of periods across the solar cycle.

A notable observation from Figure 4 is that field lines rooted in a photospheric field of larger magnitude (warmer colors in Figure 4) are always associated with very slow solar wind speeds ($v_{obs} < 400 \, \mathrm{km \, s^{-1}}$). There also appears to be a larger spread in solar wind speed among those field lines rooted in a weaker field (i.e., $|B_{ph}| < 25 \, \mathrm{G}$). To investigate this, we separated the field lines into two populations based on whether or not at least one field line in each pseudostreamer was planted in an AR. Figures 5 and 6 show the two populations of field lines separated by the pseudostreamer's source region, either entirely QS (Figure 5) or at least one AR on either side of the cusp (Figure 6). Represented in Figure 5 are 30 of the last open field lines on either side of a pseudostreamer with both footpoints rooted in QS, labeled "QS–QS" in the legend. For this subset of pseudostreamer field lines, it is apparent that several field lines have similar expansion factors (i.e., those with values between ∼5 and 25), yet the observed speed of the solar wind that emerges from those field lines varies over nearly the entire range of speeds exhibited in this study. The linear regression fit and PCC confirm that there is no statistically significant inverse correlation between observed solar wind speed and expansion factor for these field lines (Table 2).

Figure 6 shows the remaining 46 field lines and is further subdivided into two populations based on whether each field line is a part of a pseudostreamer with both footpoints in an AR (AR–AR) or a pseudostreamer with one footpoint rooted in an AR and the other in QS (AR–QS). These two populations are denoted by different shapes in Figure 6. When considering only those pseudostreamers with at least one field line footpoint planted in an AR, there is now a weak inverse correlation between f_s and v_{obs} that is approximately at the negligible

Table 2
Correlation between f_s and v_{obs}

	PCC	p-value	No. of Field Lines
Figure 4: all field lines	−0.1075	0.3552	76
Figure 5: QS–QS	0.2707	0.1479	30
Figure 6: AR–AR or AR–QS	−0.3053	0.0391	46

threshold (i.e., $0 \leqslant |\mathrm{PCC}| < 0.30$ is a negligible correlation). This correlation coefficient is, in principle, on the borderline of statistical significance because the probability of this result occurring by chance is less than 5% (i.e., a p-value <0.05 is marginally statistically significant, and a p-value <0.01 is statistically significant). However, more would have to be explored to interpret the significance of this result (see Section 4), specifically to understand why there is a weak correlation between f_s and v_{obs} for only the pseudostreamers with an AR at at least one of the two coronal hole boundaries.

4. Discussion

In this work, we test the original f_s–v_{obs} inverse relationship (Wang & Sheeley 1990) by comparing the expansion factor and observed speed of the solar wind that emerged from field lines near the open–closed boundary of coronal pseudostreamers. While it is well established that this relationship can reproduce the observed solar wind speed, on average, over large temporal scales (i.e., years, solar cycles), prior work has identified a few examples when the in situ observed pseudostreamer wind was much slower than predicted by f_s-dependent empirical relationships. With the methodology outlined in Section 2.2, we identify 38 periods when spacecraft observed the solar wind that emerged from pseudostreamers
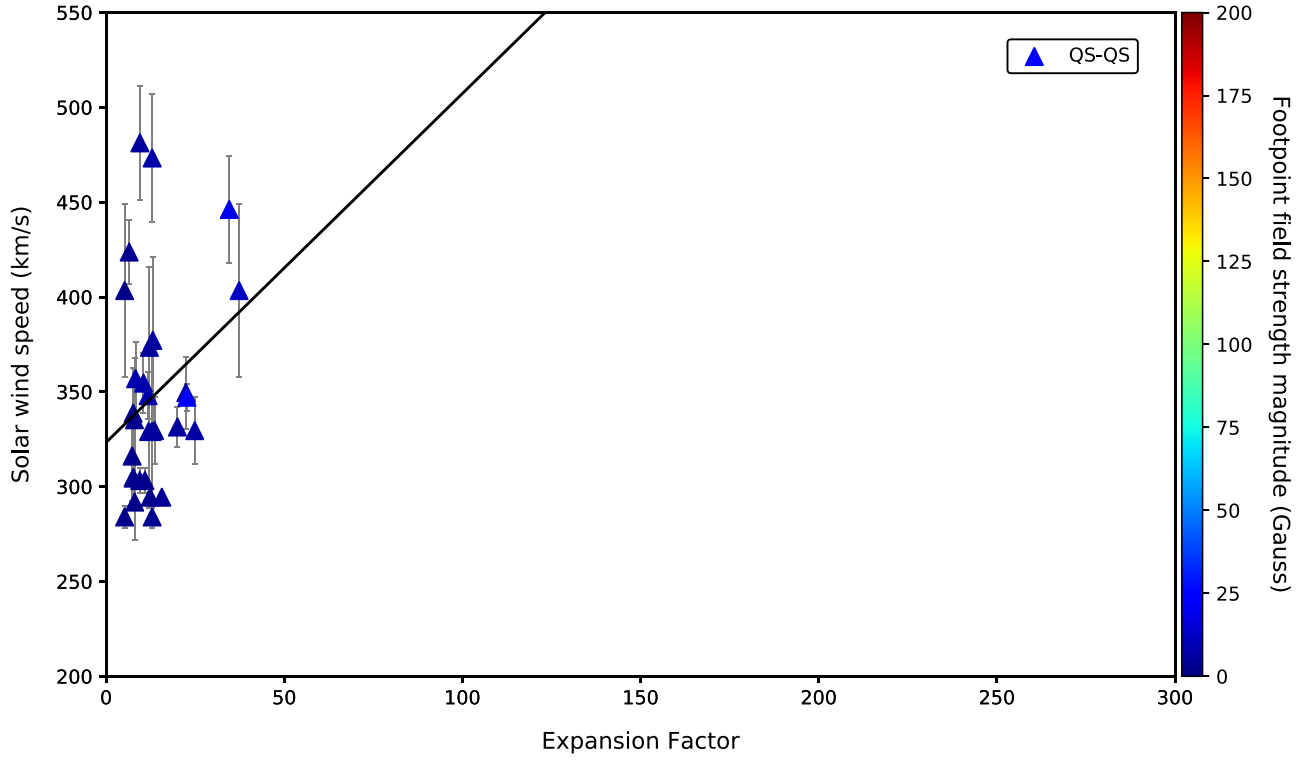
Figure 5. Observed solar wind speed vs. expansion factor for 30 individual last open field lines of 15 identified pseudostreamers. Each pseudostreamer is represented by two field lines, one from each coronal hole boundary, both of which are planted in the QS photospheric magnetic field, labeled "QS–QS" in the legend. Together, both field lines form the 2D slice of a pseudostreamer that was observed at a spacecraft. The observed solar wind speed is averaged over ±0.5 day from the WSA-derived solar wind parcel time of arrival at the spacecraft. Error bars in gray represent the standard deviation in observed solar wind speed over a 1 day bin, centered on the time (as determined by WSA) that the pseudostreamer wind was measured at each spacecraft. The black line denotes the calculated linear regression for this data set.
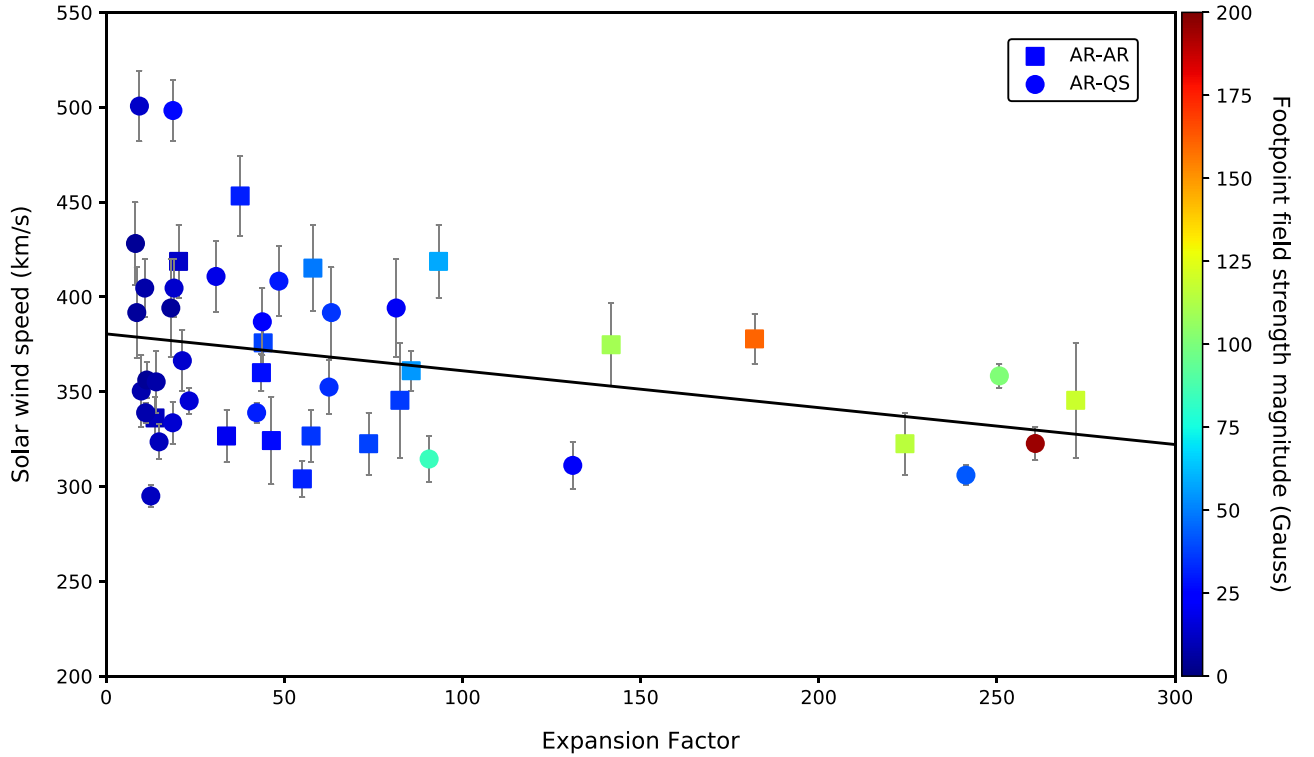

Figure 6. Observed solar wind speed vs. expansion factor for 46 individual last open field lines of 23 identified pseudostreamers. Each pseudostreamer is represented by two field lines, one from each coronal hole boundary, where at least one field line is planted in an AR. Field line populations are delineated by shape in the legend, revealing whether an individual field line belongs to a pseudostreamer with one AR and one QS footpoint (AR–QS) or a pseudostreamer with two AR footpoints (AR–AR). The observed solar wind speed is averaged over ±0.5 day from the WSA-derived solar wind parcel time of arrival at the spacecraft. Error bars in gray represent the standard deviation in observed solar wind speed over a 1 day bin, centered on the time (as determined by WSA) that the pseudostreamer wind was measured at each spacecraft. The black line denotes the calculated linear regression for this data set.
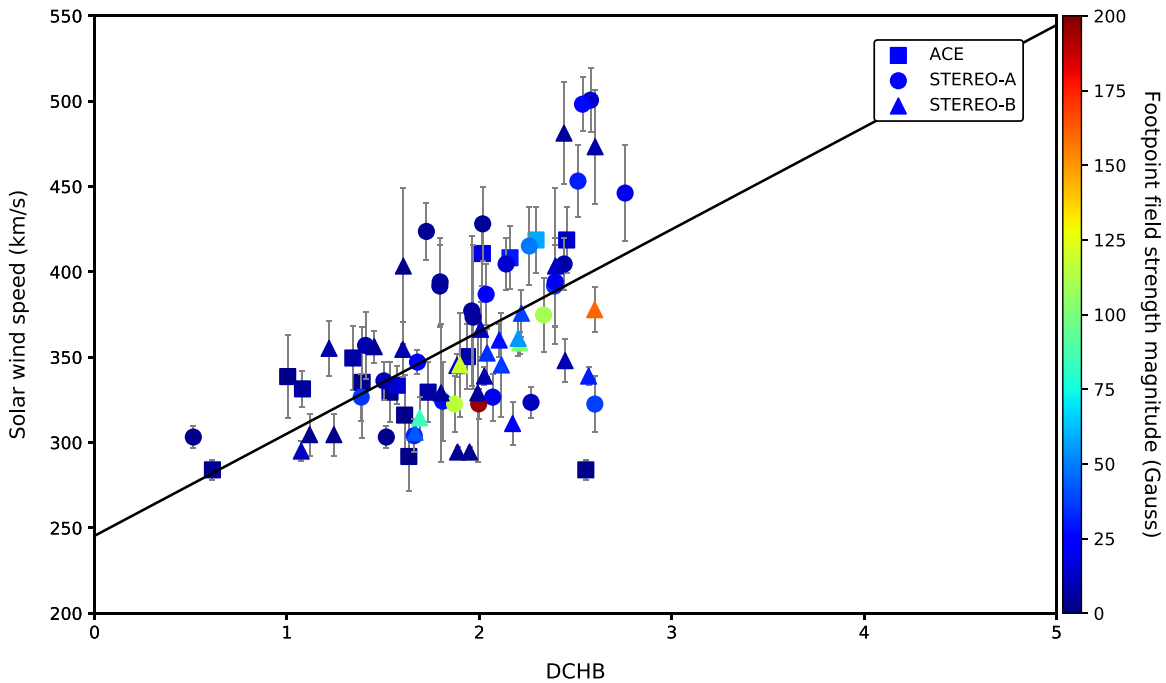
Figure 7. Same as Figure 4 but comparing observed solar wind speed with the model-derived DCHB.

from 2007 to 2016 and compared the expansion factor of the last open field lines that form these structures with the observed speed of the solar wind.

A significant result of this work is that the observed speed of the solar wind that emerged from all identified pseudostreamers is slow ($v_{obs} < 500 \, \text{km s}^{-1}$). This finding agrees with prior work and strongly suggests that the solar wind that originates from pseudostreamers is slow. Further, in all instances of testing the inverse nature of the original f_s–v_{obs} relationship for this data set, there is no strong inverse relationship between these two quantities that is statistically significant. When considering only those pseudostreamers with a QS field on either side of the cusp (Figure 5), we find that several field lines have the same expansion factor, yet the observed solar wind speed at 1 au varies over the entire range of speeds exhibited in this study. On the other hand, pseudostreamers that have at least one AR on either side of the cusp exhibit a weak, inverse relationship between f_s and v_{obs} that is marginally statistically significant (i.e., the p-value is less than 5%). However, the distribution of speed versus expansion factor seen in Figures 4–6 exhibits an envelope such that when f_s is small, a large range of speeds are observed, whereas when f_s is large, only slow wind speeds are observed. This may indicate that the expansion factor plays a role in setting an upper threshold on the observed solar wind speed.

An interesting finding of this study is the asymmetric global magnetic topology of a pseudostreamer that results from differences in the local magnetic topology at the field line footpoints of the two converging coronal hole boundaries. An example is shown in Figure 3 and Table 1, where there is an AR at one coronal hole boundary and QS at the other. We also found that field lines grounded in the largest magnitude of the photospheric field are also associated with slower solar wind, on average ($v_{obs} < 400 \, \text{km s}^{-1}$). One possibility is that the in situ observed properties of the solar wind are more dependent on the local magnetic field at the field line footpoint (e.g., AR versus QS) than the global magnetic structure (e.g.,

pseudostreamer versus helmet streamer). This hypothesis will be tested in future work and could have implications for solar wind formation theories.

While these results rigorously substantiate prior pseudostreamer case studies that have small sample sizes, it is important to note that the conclusions of this work are only applicable to pseudostreamers. Thus, we do not conclude that flux tube expansion plays no physical role in solar wind acceleration. This follows for several reasons. First, the expansion factor is calculated in this study as the rate of flux tube expansion from 1 to $2.5 \, R_\odot$, as originally defined by Wang & Sheeley (1990). However, Panasenco & Velli (2013) argued that the expansion factor as originally defined is not appropriate for pseudostreamers because field line expansion does not increase monotonically with distance from the Sun, as in helmet streamers. They proposed the use of a 3D calculation of the expansion factor to predict the solar wind speed for pseudostreamers, arguing that this quantity better captures the entire magnetic field configuration (e.g., height of the X-point, separation between corona holes). Second, recent work by Wang & Panasenco (2019) employed the use of the maximum value of the expansion factor (f_{max}) along a field line, as opposed to quantifying field line expansion from 1 to $2.5 \, R_\odot$ (Equation (1)), in an empirical relationship to determine v_{obs} for 10 different pseudostreamers observed at L1. Their results suggest that using f_{max} in lieu of f_s recovers the inverse relationship between speed and field line expansion for these pseudostreamers, though they argued that a single 2D parameter cannot fully describe the nonmonotonic expansion along the last open field lines forming pseudostreamers.

It is possible that using the traditional definition of the expansion factor (f_s) versus the maximum value (f_{max}) in our study could explain the weak inverse correlation in Figure 6 and the lack of a correlation in Figure 5. Field lines with stronger photospheric fields at their base undergo more expansion from 1 to $2.5 \, R_\odot$ that is captured by f_s. However, pseudostreamer field lines rooted in QS converge much lower down; thus, their overall expansion is not

well captured by the traditional definition of expansion factor (Equation (1)). A means of testing this theory would be to reproduce this study (i.e., Figures 4–6) using f_{max} to see if a stronger inverse relationship exists between f_{max} and v_{obs} that is statistically significant. However, it remains to be shown if replacing f_s with f_{max} in either the original WS prescription or the updated WSA relationship (Equation (2)) would reproduce the observed speed of the solar wind originating (1) from other magnetic sources (e.g., helmet streamers, coronal holes) and (2) on large temporal scales, as originally demonstrated (Wang & Sheeley 1990, Figure 3).

Third, we are comparing the observed speed of the solar wind that emerged from the last open model-derived field lines converging at a null point within the pseudostreamer. These field lines form the open–closed boundary of their respective coronal holes—an ideal environment for interchange reconnection. If interchange reconnection is an ubiquitous, time-dependent effect at the open–closed boundary, then we would expect any signature of an inverse f_s–v_{obs} relationship to be undetectable, as flux is constantly opening up and closing down. Future work will investigate this by testing if the inverse f_s–v_{obs} correlation is recovered for solar wind that (1) emerged from pseudostreamer field lines farther away from the open–closed boundary (e.g., the two to three red field lines surrounding those in green in Figure 3) or (2) the last open field lines forming helmet streamers.

Figure 7 probes the role possibly played by interchange reconnection for this set of field lines by comparing the θ_b of each pseudostreamer field line and the v_{obs} of each corresponding solar wind parcel observed in situ. Although our capacity to test this with high fidelity is limited because the grid resolution of the model is coarser than the computed resolution of θ_b, Figure 7 suggests there is a possible relationship between these two variables. First, the PCC of this data set is 0.5670, with a p-value of 10^{-7}, meaning that there is a moderate positive correlation with high statistical significance (p-value <0.01), with an extremely low probability of occurring by chance. This plot includes all of the pseudostreamer field lines in this study, whereas when the same comparison was made between f_s and v_{obs} (e.g., Figure 4), there was no correlation whatsoever. Second, although there are essentially two bins in this plot, $0° \leqslant \theta_b < 2°$ and $2° \leqslant \theta_b < 4°$, within those bins, we see that there is a smaller spread of observed speeds and lower average v_{obs} from $0° \leqslant \theta_b < 2°$. This result suggests that only the slowest wind is observed at the open–closed boundary ($\theta_b \sim 0–2°$), and solar wind that emerged farther away from this boundary (as θ_b increases) exhibits a wider range of speed. It is possible that the magnetic field near the open–closed boundary but not quite deep inside a coronal hole ($\theta_b \sim 2°–3°$) is a mixture of a continuously open field and flux tubes that are intermittently open due to interchange reconnection, resulting in a wider speed range of solar wind that emerges from this region. These preliminary conclusions will be tested in future work with 1° model resolution runs.

5. Summary

In this work, we test the original f_s–v_{obs} inverse relationship (Wang & Sheeley 1990) by performing a statistical analysis comparing the expansion factor and observed speed of the solar wind that emerged from field lines near the open–closed boundary of coronal pseudostreamers. We exploit new advances in the ADAPT–WSA model to develop a methodology to more rigorously determine the precise source region of

the in situ observed solar wind. This methodology has already been used to interpret the first observations from the Parker Solar Probe (Hill et al. 2020; Korreck et al. 2020; Nieves-Chinchilla et al. 2020; Szabo et al. 2020) and is extremely useful for coordinated multimessenger science between remote coronal and in situ solar wind observatories.

Using ADAPT–WSA, we identify 38 periods where either ACE, STEREO-A, or STEREO-B sample the solar wind that emerged from pseudostreamers. This study is the first to identify a large sample of in situ observed pseudostreamers with multiple spacecraft in order to more thoroughly investigate whether f_s-dependent empirical relationships perform poorly when pseudostreamer wind is observed in situ, as suggested by prior case studies (Riley & Luhmann 2012; Riley et al. 2015). For the 38 pseudostreamers we identified, the observed solar wind speed ranges from $\sim$280 to 500 km s^{-1}, suggesting that pseudostreamer wind is slow, on average. We also find that there is no statistically significant correlation between f_s and v_{obs} for solar wind that emerged near the open–closed boundary of pseudostreamers. This result is somewhat expected, considering we are investigating field lines near the magnetic open–closed boundary where it is likely that flux tubes are intermittently open due to interchange reconnection. Since this work does not address the vast majority of solar wind outflow along continuously open field lines, it is possible that flux tube expansion, regardless of how it is quantified (e.g., f_s, f_{max}, 3D expansion factor), could still play an important role in modulating solar wind speed for those field lines that are continuously open (i.e., deeper inside the coronal hole). If this were the case, it could explain the wider speed range exhibited as θ_b increases in Figure 7. This hypothesis will be tested in future work.

Appendix
Pseudostreamer Tables

Tables A1–A3, shown below, list all ADAPT–WSA–derived pseudostreamer field lines used in this work. Each pseudostreamer is represented by two field lines, one from each coronal hole boundary, that converge to form a pseudostreamer X-point. These two field lines mark when the spacecraft connectivity changes from one side of the pseudostreamer cusp to the other (i.e., from one coronal hole boundary to another of like polarity). In total, there are 38 pseudostreamers observed and 76 individual field lines that are the sources of the solar wind observed at either ACE, STEREO-A, or STEREO-B. The following tables also list the solar wind parcel observation times at each spacecraft that correspond to a particular field line.

Pseudostreamers are assigned an alphanumeric label in the first column of each table. Since there are two field lines associated with each pseudostreamer, the first two rows of each

Table A1
Pseudostreamers Observed at ACE

Label[a]	CR	Footpoint Coords. (Lat., Carr. Long.)	Field at 1 $R_\odot$ (AR or QS)	Date SW[b] Observed (yyyy mm dd)	s/c Time of Arrival (hh:mm:ss)	Polarity
ACE						
1a	2060	(−0.09, 345.92)	QS	2007 Aug 21	13:19:29	Inward
1a	2060	(70.73, 340.86)	QS	2007 Aug 21	13:19:38	Inward
2a	2060	(26.46, 267.77)	QS	2007 Aug 25	05:16:31	Inward
2a	2060	(6.22, 257.84)	QS	2007 Aug 25	11:18:49	Inward
1b	2061	(−2.31, 354.73)	QS	2007 Sep 16	22:37:21	Inward
1b	2061	(65.77, 356.81)	QS	2007 Sep 17	12:25:47	Inward
1 c	2062	(0.55, 6.57)	QS	2007 Nov 8	11:08:27	Inward
1 c	2062	(0.25, 5.67)	QS	2007 Nov 9	06:14:07	Inward
3a	2075	(61.61, 147.01)	QS	2008 Oct 18	04:18:03	Inward
3a	2075	(33.86, 132.12)	QS	2008 Oct 18	04:18:12	Inward
4a	2109	(−14.07, 282.85)	QS	2011 Apr 22	20:02:33	Outward
4a	2109	(11.67, 261.09)	AR	2011 Apr 22	21:46:22	Outward
5a	2109	(14.65, 258.64)	AR	2011 Apr 24	06:34:42	Outward
5a	2109	(−18.30, 220.52)	AR	2011 Apr 24	06:34:51	Outward
6	2164	(10.74, 77.86)	AR	2015 Jun 19	15:48:49	Outward
6	2164	(11.05, 55.40)	QS	2015 Jun 20	01:19:03	Outward

Notes.
[a] Each unique pseudostreamer is assigned a number in this table. If a pseudostreamer was observed at more than one spacecraft or in another rotation (even if several rotations ahead), a letter is assigned. In some cases, the same pseudostreamer is observed several rotations later, after significant evolution has occurred.
[b] Solar wind.

Table A2
Pseudostreamers Observed at STEREO-A

Label[a]	CR	Footpoint Coords. (Lat./Carr. Long.)	Field at 1 $R_\odot$ (AR or QS)	Date SW[b] Observed (yyyy mm dd)	s/c Time of Arrival (hh:mm:ss)	Polarity
STEREO-A						
2b	2060	(50.97, 250.96)	QS	2007 Aug 26	12:11:23	Inward
2b	2060	(−2.89, 241.52)	QS	2007 Aug 26	13:05:14	Inward
2 c	2062	(61.11, 261.96)	QS	2007 Oct 18	07:46:51	Inward
2 c	2062	(18.44, 251.51)	QS	2007 Oct 18	07:47:00	Inward
7a	2100	(33.93, 154.84)	QS	2010 Sep 5	09:55:09	Inward
7a	2100	(25.66, 108.46)	AR	2010 Sep 5	09:55:26	Inward
8	2101	(−13.65, 193.77)	QS	2010 Sep 29	11:51:30	Inward
8	2101	(14.61, 180.37)	QS	2010 Sep 30	13:22:48	Inward
9a	2109	(13.29, 315.38)	AR	2011 Apr 29	01:39:39	Outward
9a	2109	(7.51, 273.23)	AR	2011 Apr 29	20:09:01	Outward
5b	2109	(14.53, 258.35)	AR	2011 May 3	20:38:15	Outward
5b	2109	(−18.14, 219.19)	AR	2011 May 3	20:38:24	Outward
9b	2110	(18.69, 312.88)	AR	2011 May 27	04:54:20	Outward
9b	2110	(15.51, 260.24)	AR	2011 May 27	14:15:30	Outward
10	2110	(12.88, 127.30)	AR	2011 Jun 10	03:31:58	Inward
10	2110	(37.59, 80.02)	QS	2011 Jun 10	03:32:07	Inward
11a	2112	(0.12, 168.82)	QS	2011 Aug 1	00:55:44	Inward
11a	2112	(−20.44, 116.91)	AR	2011 Aug 1	14:12:55	Inward
11b	2113	(3.36, 168.76)	QS	2011 Aug 28	15:45:56	Inward
11b	2113	(−22.99, 113.56)	AR	2011 Aug 28	15:46:05	Inward
12a	2113	(17.10, 64.95)	AR	2011 Sep 4	10:53:28	Inward
12a	2113	(19.18, 28.26)	AR	2011 Sep 4	10:53:37	Inward
13	2116	(−14.65, 95.57)	AR	2011 Nov 21	16:01:12	Inward
13	2116	(8.99, 65.91)	AR	2011 Nov 22	05:23:43	Inward
14	2136	(29.35, 244.20)	QS	2013 May 11	15:03:27	Inward
14	2136	(20.47, 212.81)	AR	2013 May 11	19:44:41	Inward
15a	2136	(28.64, 123.39)	QS	2013 May 23	10:22:39	Outward
15a	2136	(30.18, 102.12)	QS	2013 May 23	19:24:14	Outward
16	2152	(−9.12, 320.18)	QS	2014 Jul 17	10:03:04	Outward
16	2152	(−10.99, 273.15)	AR	2014 Jul 17	12:56:44	Outward

Notes.
[a] Each unique pseudostreamer is assigned a number in this table. If a pseudostreamer was observed at more than one spacecraft or in another rotation (even if several rotations ahead), a letter is assigned. In some cases, the same pseudostreamer is observed several rotations later after significant evolution has occurred.
[b] Solar wind.

Table A3
Pseudostreamers Observed at STEREO-B

Label[a]	CR	Footpoint Coords. (Lat./Carr. Long.)	Field at 1 $R_\odot$ (AR or QS)	Date SW[b] Observed (yyyy mm dd)	s/c Time of Arrival (hh:mm:ss)	Polarity
STEREO-B						
2d	2060	(50.79, 250.65)	QS	2007 Aug 24	12:52:25	Inward
2d	2060	(−2.89, 243.63)	QS	2007 Aug 24	12:52:34	Inward
2e	2064	(57.53, 290.82)	QS	2007 Dec 8	22:36:03	Inward
2e	2064	(14.02, 260.21)	QS	2007 Dec 8	22:36:12	Inward
2f	2065	(60.95, 322.81)	QS	2008 Jan 2	20:41:51	Inward
2f	2065	(13.70, 325.59)	QS	2008 Jan 2	20:42:00	Inward
3b	2076	(32.77, 119.62)	AR	2008 Nov 15	09:21:19	Inward
3b	2076	(56.09, 112.70)	QS	2008 Nov 15	20:50:30	Inward
7b	2100	(31.92, 157.94)	QS	2010 Aug 25	21:49:32	Inward
7b	2100	(24.76, 108.77)	AR	2010 Aug 25	23:13:47	Inward
7 c	2101	(29.67, 145.69)	QS	2010 Sep 20	00:46:39	Inward
7 c	2101	(20.42, 114.29)	QS	2010 Sep 20	02:24:00	Inward
17	2107	(26.27, 167.79)	AR	2011 Mar 1	21:24:55	Inward
17	2107	(37.54, 150.30)	AR	2011 Mar 2	01:15:53	Inward
18	2107	(20.93, 135.75)	AR	2011 Mar 4	07:56:04	Inward
18	2107	(16.66, 111.79)	QS	2011 Mar 4	07:56:12	Inward
4b	2109	(−12.97, 283.38)	QS	2011 Apr 15	23:47:02	Outward
4b	2109	(11.17, 262.91)	AR	2011 Apr 16	19:48:35	Outward
11 c	2113	(−0.48, 169.62)	QS	2011 Aug 13	23:44:10	Inward
11 c	2113	(−24.79, 115.26)	QS	2011 Aug 13	23:44:18	Inward
12b	2113	(16.55, 64.93)	AR	2011 Aug 20	15:54:52	Inward
12b	2113	(19.01, 28.24)	AR	2011 Aug 20	15:55:00	Inward
19a	2120	(35.03, 289.95)	QS	2012 Feb 9	08:14:47	Inward
19a	2120	(18.46, 238.15)	AR	2012 Feb 9	12:31:58	Inward
19b	2121	(21.64, 289.26)	AR	2012 Mar 7	03:13:24	Inward
19b	2121	(19.15, 242.78)	AR	2012 Mar 7	05:41:25	Inward
15b	2138	(−13.51, 132.65)	AR	2013 Jun 25	09:23:20	Outward
15b	2138	(30.07, 101.06)	QS	2013 Jun 26	04:03:13	Outward
15 c	2139	(16.99, 54.44)	QS	2013 Jul 23	22:07:32	Outward
15 c	2139	(11.32, 53.40)	QS	2013 Jul 24	09:48:40	Outward

Notes.

[a] Each unique pseudostreamer is assigned a number in this table. If a pseudostreamer was observed at more than one spacecraft or in another rotation (even if several rotations ahead), a letter is assigned. In some cases, the same pseudostreamer is observed several rotations later after significant evolution has occurred.
[b] Solar wind.

table and every proceeding pair of rows share the same alphanumeric label. Each unique pseudostreamer is first assigned a number. If this same structure has either been observed at a different spacecraft or resampled by the same spacecraft in another rotation, it is marked with a letter following the reference number. In either scenario, the pseudostreamer undergoes evolution, and the spacecraft sample a different 2D slice of the 3D structure. For example, labels of 1a and 1b would be two different samples in time and space of the "same" pseudostreamer.

ORCID iDs

Samantha Wallace ● https://orcid.org/0000-0002-1091-4688
Nicholeen Viall ● https://orcid.org/0000-0003-1692-1704
Ylva Pihlström ● https://orcid.org/0000-0003-0615-1785

References

Altschuler, M. D., & Newkirk, G. 1969, SoPh, 9, 131
Arge, C. N., Henney, C. J., Hernandez, I. G., et al. 2013, in AIP Conf. Ser. 13, Solar Wind CS-1539, ed. G. P. Zank et al. (Melville, NY: AIP), 11
Arge, C. N., Henney, C. J., Koller, J., et al. 2010, in AIP Conf. Ser. 12, Solar Wind CS-1216, ed. M. Maksimovic et al. (Melville, NY: AIP), 343
Arge, C. N., Henney, C. J., Koller, J., et al. 2011, in ASP Conf. Ser. 5, Numerical Modeling of Space Plasma Flows, ed. N. V. Pogorelov, E. Audit, & G. P. Zank (San Francisco, CA: ASP), 99
Arge, C. N., Luhmann, J. G., Odstrcil, D., Schrijver, C. J., & Li, Y. 2004, JASTP, 66, 1295
Arge, C. N., Odstrcil, D., Pizzo, V. J., & Mayer, L. R. 2003, in AIP Conf. Ser. CS-679, Solar Wind, ed. M. Velli et al. (Melville, NY: AIP), 190
Arge, C. N., & Pizzo, V. J. 2000, JGR, 105, 10465
Cranmer, S. R. 2009, Living Rev. Solar Phys., 6, 3
Cranmer, S. R. 2010, ApJ, 710, 676
Cranmer, S. R., van Ballegooijen, A. A., & Edgar, R. J. 2007, ApJS, 171, 520
Crooker, N. U., Antiochos, S. K., Zhao, X., & Neugebauer, M. 2012, JGRA, 117, 4104
de Toma, G., Arge, C. N., & Riley, P. 2005, in Proc. Solar Wind 11/SOHO 16, Connecting Sun and Heliosphere (ESA SP-592), ed. B. Fleck, T. H. Zurbuchen, & H. Lacoste (Paris: ESA), 609
Feldman, U., Doschek, G. A., Mariska, J. T., Bhatia, A. K., & Mason, H. E. 1978, ApJ, 226, 674
Fisk, L. A. 2003, JGRA, 108, 1157
Geiss, J., Gloeckler, G., & von Steiger, R. 1995, SSRv, 72, 49
GeospaceX 2015, Software developed by AER, Inc. under contract to Air Force Research Laboratory, Space Weather Division
Henney, C. J., Keller, C. U., Harvey, J. W., et al. 2009, in ASP Conf. Ser. 5, Solar Polarization CS-405, ed. S. V. Berdyugina, K. N. Nagendra, & R. Ramelli (San Francisco, CA: ASP), 47
Hickmann, K. S., Godinez, H. C., Henney, C. J., & Arge, C. N. 2015, SoPh, 290, 1105
Hill, M., Mitchell, D., Allen, R., et al. 2020, ApJS, 246, 65

Hoeksema, J. T., Wilcox, J. M., & Scherrer, P. H. 1983, JGR, 88, 9910
Korreck, K., Szabo, A., Chinchilla, T., et al. 2020, ApJS, 246, 69
Nieves-Chinchilla, T., Szabo, A., Korreck, K., et al. 2020, ApJS, 246, 63
Owens, M. J., Arge, C. N., Spence, H. E., & Pembroke, A. 2005, JGRA, 110, A12105
Panasenco, O., & Velli, M. 2013, in AIP Conf Proc. 1539, Solar Wind 13, 1539 (Melville, NY: AIP), 50
Pizzo, V., Millward, G., Parsons, A., et al. 2011, SpWea, 9, 3004
Richardson, I. G. 2014, SoPh, 289, 3843
Riley, P., Linker, J. A., & Arge, C. N. 2015, SpWea, 13, 154
Riley, P., Linker, J. A., & Mikić, Z. 2001, JGRA, 106, 15889
Riley, P., & Luhmann, J. G. 2012, SoPh, 277, 355
Schatten, K. H. 1971, CosEl, 2, 232
Schatten, K. H., Wilcox, J. M., & Ness, N. F. 1969, SoPh, 6, 442
Schrijver, C. J., & de Rosa, M. L. 2003, SoPh, 212, 165
Schwadron, N., Fisk, L., & Zurbuchen, a. 1999, ApJ, 521, 859
Sheeley, N. R. 2017, HGSS, 8, 21
Szabo, A., Larson, D., Whittlesey, P., et al. 2020, ApJS, 246, 47
Viall, N. M., & Borovsky, J. 2020, JGR Space Physics, e2018JA026005
Wallace, S., Arge, C. N., Pattichis, M., Hock-Mysliwiec, R. A., & Henney, C. J. 2019, SoPh, 294, 19
Wang, Y.-M., Grappin, R., Robbrecht, E., & Sheeley, N. R., Jr. 2012, ApJ, 749, 182
Wang, Y.-M., Hawley, S. H., & Sheeley, N. R., Jr. 1996, Sci, 271, 464
Wang, Y.-M., Ko, Y.-K., & Grappin, R. 2009, ApJ, 691, 760
Wang, Y.-M., & Panasenco, O. 2019, ApJ, 872, 139
Wang, Y.-M., & Sheeley, N., Jr. 2003, ApJ, 587, 818
Wang, Y.-M., & Sheeley, N. R., Jr. 1990, ApJ, 355, 726
Wang, Y.-M., & Sheeley, N. R., Jr. 1992, ApJ, 392, 310
Wang, Y.-M., & Sheeley, N. R., Jr. 1995, ApJL, 447, L143
Wang, Y.-M., Sheeley, N. R., Jr., & Rich, N. B. 2007, ApJ, 658, 1340
Worden, J., & Harvey, J. 2000, SoPh, 195, 247
Zurbuchen, T. H., Fisk, L. A., Gloeckler, G., & Schwadron, N. A. 1998, SSRv, 85, 397